Chain-Walking Polymerization of α-Olefins by α-Diimine Ni(II) Complexes: Effect of Reducing the Steric Hindrance of *Ortho*- and *Para*-Aryl Substituents on the Catalytic Behavior, Monomer Enchainment, and Polymer Properties

Ivana Pierro,[†,‡] Giorgia Zanchin,[†,§] Emilio Parisini,[∥] Javier Martí-Rujas,[∥] Maurizio Canetti,[†] Giovanni Ricci,[†] Fabio Bertini,*[,†] and Giuseppe Leone*[,†]

[†]CNR-Istituto per lo Studio delle Macromolecole (ISMAC), via A. Corti 12, I-20133 Milano, Italy
[‡]Dipartimento di Scienze Chimiche, Università degli Studi di Napoli Federico II, Complesso Monte S. Angelo, Via Cintia, I-80126 Napoli, Italy
[§]Dipartimento di Chimica, Università degli Studi di Milano, via C. Golgi 19, I-20133 Milano, Italy
[∥]Center for Nano Science and Technology at Polimi, Istituto Italiano di Tecnologia, Via Pascoli 70/3, I-20133 Milano, Italy

With Brookhart type α-diimine Ni(II) based catalysts, it is highly challenging to tune polymers branching level and branch-type distribution, which in turn strongly affects thermal and mechanical properties, through the aryl *ortho*-positions modification, while maintaining high turnover frequencies (TOFs). Herein, we are interested in performing a systematic investigation on the polymerization of 1-octene, 1-decene, and 1-octadecene catalyzed by a series of α-diimine nickel(II) complexes with methyl ligand backbone and different substituents in aryl positions (**Ni1**−**Ni6**). In addition to bulky isopropyl and *tert*-butyl substituents described in the original Brookhart's work, complexes with different aryl *ortho*- and *para*-substituted α-diimine ligands, including the less sterically demanding methyl and ethyl substituents, are investigated. The ^{13}C NMR spectra of the polymers have been assigned in detail, and some unique features have been identified and related to the chain-walking coordination/insertion mechanism. Changes in the ligand structure and monomer size have important effects on the numerous combinations of insertion and chain-walking paths from which different branches are installed. We have also carried out a comprehensive investigation of the mechanical behavior of the polymers by means of uniaxial stretching until failure, step-cycle, and creep tensile tests. Overall, the resulting polymers exhibited a broad spectrum of tensile properties, depending on their microstructure and crystallinity which in turn are strongly affected by monomer length and type of α-diimine ligand. 1-Octene and 1-decene polymers behave as elastomers with excellent mechanical properties, i.e., high elongation at break (up to 2000%) and good strain recovery, while 1-octadecene polymers behave as plastomers.

INTRODUCTION

Long chain α-olefins are abundant, inexpensive, versatile monomers manufactured from the oligomerization of ethylene,[1] Fischer−Tropsch synthesis,[2] and catalytic processes from ethanol.[3] These monomers are commonly used as comonomers for the production of HDPE and LLDPE.[4] Polymer chemists in academia and industry have invested considerable attention and efforts in finding alternatives to thermoset elastomers from α-olefins. Polyolefin thermoplastic elastomers (TPEs) are an important class of materials with applications ranging from packaging to lightweight engineering plastics for automotive, textiles, rubbers, sporting goods, and electrical and thermal insulation.[5−12] The global TPEs demand will grow in the coming years, and part of this growth comes from applications where TPEs have directly displaced more traditional thermoset, vulcanized rubbers. TPEs combine the processing advantages (i.e., they can be processed by injection molding, extrusion, and blow molding) and recycling potential of thermoplastics with the flexibility, low modulus, and soft touch of elastomers.[13,14] A two-phase molecular structure usually gives TPEs their combination of strength and flexibility: amorphous domains in the polymer are soft and provide its elastomeric nature, while the hard crystalline segments, usually dispersed throughout the amorphous matrix, form physical cross-links that give tensile strength, resistance to chemicals, and produce recoverable elasticity after strain-induced deformation.[15] Physical properties and elasticity of TPEs strongly depend on the distribution of

This document is the Accepted Manuscript version of a Published Work that appeared in final form in Macromolecules 2018, 51, 801-814, copyright © American Chemical Society after peer review and technical editing by the publisher. To access the final edited and published work see http://dx.doi.org/10.1021%2Facs.macromol.7b02242

crystalline and amorphous regions and polymer microstructure.[16−18]

Polyolefin TPEs can be obtained through the copolymerization of ethylene with α-olefins catalyzed by a metallocene catalyst.[19] Elsewhere, late-transition-metal catalysts have shown great potential in their ability to afford branched and hyperbranched polymer that are related in structure to TPEs. A milestone in this field was the discovery of α-diimine Ni(II) and Pd(II) complexes by Brookhart in the 1990s.[20] Indeed, the application of these complexes allowed the synthesis of branched polymers[21−27] and block copolymers containing semicrystalline hard segments and amorphous soft blocks, which offer mechanical stability and flexibility, respectively, and may have interesting applications as TPEs.[28−32]

The striking feature of α-diimine Ni(II) and Pd(II) complexes is the chain-walking mechanism, which involves β−H elimination followed by metal hydride reinsertion into the growing polymer chain with opposite regiochemistry. The active site "walks" on the growing polymer chain during the propagation step so that the new incoming monomer is assembled onto the polymer backbone rather than at the end, giving branched polymers (Scheme 1).[20,33]

Scheme 1. Mechanism for Ethylene Polymerization and α-Olefin Enchainment (Mt = Ni, Pd; NN = Diimine Ligand; CW = Chain-Walking; *ins* = New Further Insertion)

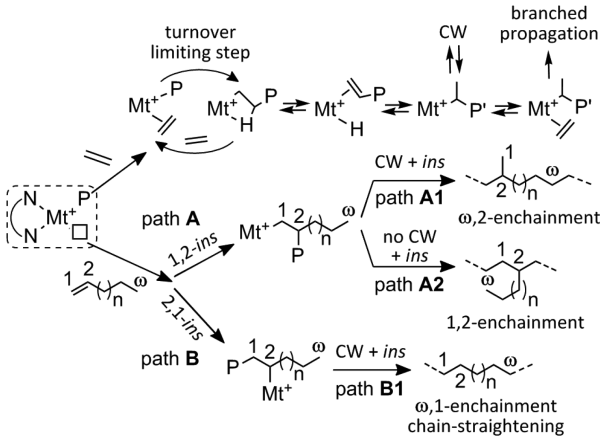

Moreover, when the polymerization involves α-olefins with high number of carbon atoms, a different enchainment becomes competitive: a significant fraction of monomer insertions occurs in a 2,1 manner, followed by chain-walking to the terminal ω carbon of the growing chain before successive monomer insertion. The result of this ω,1-enchainment is the placement of longer linear methylene sequences (Scheme 1, path B).[34−36] The competition between chain propagation and chain-walking, which are intrinsically associated with the regiochemistry of insertion, is the major factor determining the branching density and branch-type distribution, which in turn are key parameters that greatly dictate the polymer properties.

Since Brookhart's initial work (Chart 1, **I**),[37] impressive efforts have been made to improve the overall understanding of these systems[20,38,39] and to control the regiochemistry of olefin insertion, mainly through the aryl *ortho*-positions modification (Chart 1, **I**−**III**) including steric tuning and electronic perturbations[40−42] and ligand backbone adjustments (Chart 1, **V** and **VI**).[43,44] The *ortho*-aryl groups are prone to easy chemical modification and exert a significant influence on the polymerization activities as well as on the thermal stability.[42,43,45] In addition, the alkyl substitution of N−aryl groups exerts a precise control over both the regiochemistry of olefin insertion and the location of the incoming monomer after chain-walking. By modifying the ligand structure, the various combinations of monomer insertion and chain-walking give rise to highly branched polymers with low melting temperature and crystallinity (Scheme 1, path A) or chain-straightened PE-like materials with high melting temperature and crystallinity (Scheme 1, path B).[32,41]

A series of α-diimine Ni(II) complexes with a variety of electron-donating and electron-withdrawing substituents on the *para* positions of the bis-aryl ligand have been also synthesized and used for the polymerization of olefins.[46−49] The presence of substituents on the *para* positions strongly perturbs the metal electronics and exerts a significant impact on the catalyst's stability, lifetime, and polymer molecular weight and topology.

More recently, complexes of type **IV**, in which 8-arylnaphthyl-α-diimine positions the aryl groups over the axial sites to form "sandwich" type complexes, have been

Chart 1. Some α-Diimine Ligand Structures Reported in the Literature and α-Diimine Ni(II) Complexes Used in This Work

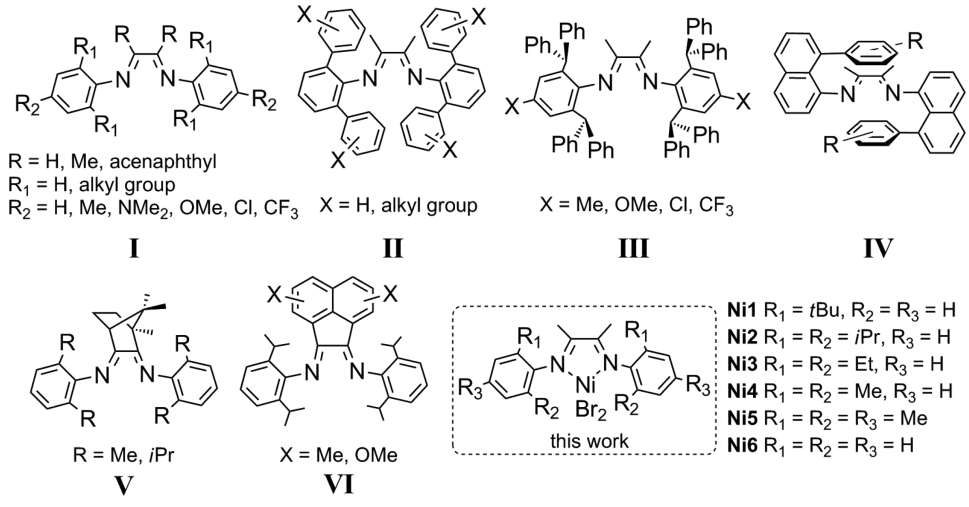

reported.[39,41,50] It has been demonstrated that these bulky substituents are more effective in shielding the axial sites than the *ortho*-isopropyl groups in complexes of type **I** (Chart 1). These sandwich catalysts produced highly branched ultrahigh molecular weight PEs[50] and chain-straightened poly(α-olefin)s with the highest melting temperatures reported to date.[39,41]

The evolution of α-diimine Ni(II) complexes has been accompanied by a progressive increase of steric bulk and number of *ortho*-substituents. This is because the *ortho*-substituents offer steric crowding both above and below the metal center and this steric hindrance at the axial sites is critical for suppressing the associative chain-transfer process.[20,46] It has been demonstrated that by modifying the *ortho*-substituents from methyl to isopropyl, the complex bearing the bulkier isopropyl group affords much higher molecular weight polymers at significantly higher polymerization activity than the corresponding methyl-substituted complexes.[20,24,51−53] Thus, it is generally accepted that a key feature for producing high polymers with high turnover frequencies lies in the suppression of chain transfer by the steric bulk of the *ortho*-aryl substituents. However, this is well demonstrated for the polymerization of ethylene, while no systematic investigation of the effect of *ortho* substitution in α-diimine Ni(II) complexes, especially including low sterically demanding *ortho*-aryl substituents, on the polymerization of α-olefins has ever been reported.

In this work, we performed a systematic investigation on the polymerization of 1-octene, 1-decene, and 1-octadecene catalyzed by traditional α-diimine Ni(II) complexes with methyl α-diimine backbone and different aryl *ortho*- (H, Me, Et, *i*Pr, *t*Bu) and *para*- (H, Me) substituents (Chart 1, **Ni1− Ni6**). We focused our attention on this class of complexes because in comparison with those having acenaphthyl α-diimine backbone, α-diimine Ni(II) complexes with methyl α-diimine backbone gave higher molecular weight polymers and enhanced activity.[46] The effect of ligand steric and electronic perturbation on the catalytic behavior, monomer enchainment, and polymer properties is discussed. The mechanical properties of the resulting polymers are thoroughly explored by uniaxial tension until failure, step-cycle, and creep tensile tests. In addition, the crystal structures of **Ni3−Ni6** are reported.

EXPERIMENTAL SECTION

Materials. Manipulations of air- and/or moisture-sensitive materials were carried out under an inert atmosphere using a dual vacuum/nitrogen line and standard Schlenk-line techniques. Toluene (Aldrich, >99.5%) was refluxed over Na for 8 h and then distilled and stored over molecular sieves under nitrogen. Diethylaluminum chloride (Et_2AlCl, Aldrich) was used as received. 1-Octene (Aldrich, 98%) and 1-decene (Aldrich, ≥97%) were refluxed over CaH_2 for 4 h, then distilled via trap-to-trap, and finally stored under nitrogen and kept at −18 °C. 1-Octadecene (Aldrich, ≥95%) was degassed under vacuum then by bubbling nitrogen, kept over molecular sieves and used without any further purification. Deuterated solvent for NMR measurements ($C_2D_2Cl_4$) (Cambridge Isotope Laboratories, Inc.) was used as received. **Ni1−Ni6** (Chart 1) were synthesized according to the literature.[37] Single crystal, suitable for X-ray structure determination, was obtained for **Ni3−Ni6** from a cold CH_2Cl_2 solution.

General Polymerization Procedure. Polymerization was carried out in a 25 mL round-bottomed Schlenk flask. The reactor was first dried by heating at 110 °C, and then vacuum was applied for 1 h. Toluene, the monomer, Et_2AlCl (200 equiv to Ni), and a toluene solution of the nickel complex (2 mg/mL) were transferred into the reactor vessel in that order. Polymerization was quenched with methanol containing a small amount of hydrochloric acid. The precipitated polymer was collected by filtration, repeatedly washed with fresh methanol, and then dried to constant weight. 1-Octadecene polymers were then extracted with acetone through the Soxhlet method for 12 h to remove the unreacted monomer.

Single Crystal X-ray Diffraction Data. The diffraction data were collected at room temperature for **Ni3−Ni5** and at 100 K for **Ni6** using a Bruker X8 Prospector APEX-II/CCD diffractometer equipped with a focusing mirror (Cu Kα radiation, λ = 1.541 78 Å). The structures were determined using direct methods and refined (based on F^2 using all independent data) by full-matrix least-squares methods (SHELXTL 97).[54,55] All non-hydrogen atoms were located from different Fourier maps and refined with anisotropic displacement parameters. Hydrogen atoms were added in riding positions.

Polymer Characterization. For ^{13}C NMR, about 100 mg of polymer was dissolved in $C_2D_2Cl_4$ in a 10 mm tube. HDMS (hexamethyldisiloxane) was used as internal chemical shift reference. The spectra were recorded on a Bruker NMR AVANCE 400 spectrometer operating at 100.58 MHz (^{13}C) in the PFT mode working at 103 °C. The applied conditions were the following: 10 mm probe, 90° pulse angle; 64K data points; acquisition time 5.56 s; relaxation delay 20 s; 3−4K transient. Proton broad-band decoupling was achieved with a 1D sequence using bi_waltz_16_32 power-gated decoupling. ^1H NMR spectroscopy was used to determine overall branching.[40] The fraction of ω,1-insertions was calculated from the equation reported by Brookhart.[34] ^{13}C NMR spectroscopy was used to examine the types of branches. The quantitative analysis was based on the equations reported by Galland.[56] The molecular weight-average (M_n) and the molecular weight distribution (M_w/M_n) were obtained by a high temperature Waters GPCV2000 size exclusion chromatography (SEC) system using an online refractometer detector. The experimental conditions consisted of three PL Gel Olexis columns, *o*-dichlorobenzene as the mobile phase, 0.8 mL/min flow rate, and 145 °C. The calibration of the SEC system was constructed using 18 narrow M_w/M_n poly(styrene) standards with molar weights ranging from 162 to 5.6 × 10^6 g/mol. For SEC analysis, about 12 mg of polymer was dissolved in 5 mL of *o*-DCB with 0.05% of BHT as antioxidant. Differential scanning calorimetry (DSC) measurements were performed on a PerkinElmer DSC 8000 instrument equipped with a liquid nitrogen device. The scans were carried out from −100 to 130 °C under a nitrogen atmosphere using heating and cooling rates of 20 °C/min. Crystallinity (X_{DSC}) was calculated from the DSC scans as follows: $X_{DSC} = (\Delta H_f/\Delta H_0) \times 100$, where ΔH_f is the enthalpy associated with the melting of the sample and ΔH_0 is the melting enthalpy of a 100% crystalline poly(ethylene) taken equal to 290 J/g.[57] Wide-angle X-ray diffraction (WAXD) data were obtained at 18 °C using a Siemens D-500 diffractometer equipped with a Siemens FK 60-10 2000 W tube (Cu Kα radiation, λ = 0.154 nm). The operating voltage and current were 40 kV and 40 mA, respectively. The data were collected from 5 to 35 2θ° 0.02 2θ° intervals. Small-angle X-ray scattering (SAXS) measurements were conducted at 18 °C with a Kratky compact camera. Monochromatized Cu Kα radiation (λ = 0.154 nm) was supplied by a stabilized Siemens Krystalloflex 710 generator and a Siemens FK 60-10 2200 W Cu target tube operated at 40 kV and 40 mA. The scattered intensity was counted in different ranges of 2θ° by using a step scanning proportional counter with pulse height discrimination, the abscissa variable was $h = \sin(\theta)\ 4\pi/\lambda$, and the data were successively corrected for blank scattering and desmeared. The materials for structural and mechanical characterization were molded in a press at 90 °C (1-octene and 1-decene polymers) or 110 °C (1-octadecene polymers) and 50 bar for 5 min; then the press plates were cooled at 20 °C/min to room temperature. Films with a thickness of about 150 μm were produced. Tensile dog-bone-shaped specimens (length overall 75 mm, gauge length 25 mm, and width of narrow section 4 mm) were analyzed at 20 °C using a Zwick Roell ProLine Z010 mechanical tester equipped with a XforceP (50 N) load cell at a constant crosshead rate of 15 mm/min. In the hysteresis experiments performed at the fixed strain of 300% or a gradually increased strain between 30 and 1750%, the specimens were cyclically loaded and unloaded in uniaxial tension. The strain recovery (SR) was calculated as SR = 100($\varepsilon_a - \varepsilon_r$)/$\varepsilon_a$, where ε_a is the applied

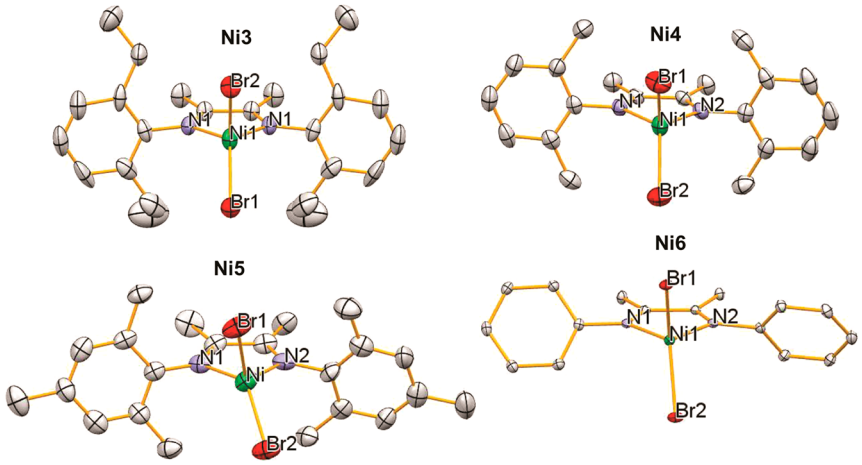

Figure 1. X-ray crystal structure for **Ni3**–**Ni6**. Hydrogen atoms are omitted for clarity. Atoms are drawn at the 30% probability level.

strain and ε_r is the strain in the cycle at zero load after the applied strain. For each material, at least five samples were tested for extension experiments and two samples for strain recovery tests.

RESULTS AND DISCUSSION

Synthesis and X-ray Crystallography of Nickel Complexes. Nickel complexes were synthesized using a known procedure.[39] The reaction of ligands with 1 equiv of (DME)$NiBr_2$ (DME = 1,2-dimethoxyethane) in CH_2Cl_2 afforded the desired **Ni1**–**Ni6** complexes as mustard and brown solids at 80–93% yields. Crystallization of **Ni3**–**Ni6** from CH_2Cl_2 at low temperature afforded crystals suitable for single crystal X-ray diffraction. ORTEP diagrams for these four compounds are depicted in Figure 1, while crystal data, data collection, and refinement parameters are listed in the Supporting Information. Numerous attempts to obtain single crystals of **Ni1** suitable for X-ray diffraction analysis failed, while the molecular structure of **Ni2** is published in ref 58.

Complex **Ni3** crystallized in the orthorhombic space group *Pnma*, as that reported in the literature for **Ni2**,[58] while **Ni4** crystallized in the monoclinic space group *C*2/*c*, **Ni5** in the monoclinic space group $P2_1/c$, and **Ni6** in the orthorhombic space group $P2_12_12_1$. As shown in Figure 1, all the complexes have similar structure; that is, the distorted tetrahedral geometry at the nickel center is composed of the two nitrogen atoms and two bromine atoms. The observed bond lengths are typical for α-diimine Ni(II) complexes.[24,42,58] The C═N imine (1.27(1)Å for **Ni3**, 1.30(1)Å for **Ni4**, 1.25(2) and 1.28(2)Å for **Ni5**, 1.290(5) and 1.291(5)Å for **Ni6**) and the N–C_{aryl} bonds (1.43(1)Å for **Ni3**, 1.454(9) and 1.441(9)Å for **Ni4**, 1.46(3) and 1.42(2)Å for **Ni5**, 1.425(5) and 1.435(5) Å for **Ni6**) are in agreement with the expected lengths for this type of bond.[59]

For disubstituted complexes, the dihedral angle formed by the planes containing the atoms N1–Ni–N2 and Br1–Ni–Br2 is 90° for **Ni3**, 86.67° for **Ni4**, and 86.62° for **Ni6**. Thus, the plane of the aryl ring becomes more rigidly locked perpendicular to the coordination plane with increasing the steric bulk of the *ortho* substituents.[60] In addition, the X-ray structure analysis of **Ni5** shows that the presence of a methyl in the *para* position has a significant influence on the coordination geometry, changing the dihedral angle formed by the planes containing the atoms N1–Ni–N2 and Br1–Ni–Br2 to 78.76°, thus suggesting that the introduction of groups in the *para* position causes repulsive interactions between substituents. Similar characteristics were observed in similar Ni(II) complexes bearing 4,5-bis(arylimino)pyrenylidenes.[47] The dihedral angle formed by the two imino-phenyl rings is 20.61° for **Ni3**, 11.66° for **Ni4**, 22.23° for **Ni5**, and 65.38° for **Ni6**. This confirms that the absence of *ortho* substituents has a strong influence on the steric environment, allowing a higher degree of freedom for the rotation of the aniline moieties, and hence no steric hindrance at the axial sites of the nickel center. As it will be discussed later, this is the reason why **Ni6** is not active in the polymerization.

Polymerization of α-Olefins. All the complexes were used, in combination with Et_2AlCl, in the polymerization of 1-octene, 1-decene, and 1-octadecene. A short polymerization time was chosen for the initial screening because of the ease in maintaining homogeneous conditions, avoiding mass transfer limitation due to the formation of insoluble polymer, and insufficient mixing. In this way, the observed differences in turnover frequencies (TOFs) can only be ascribed to the ligand alkyl substituent effects. The results are summarized in Table 1.

Ni2–**Ni5** were highly active in the polymerization of higher α-olefins, TOF being in the range of 200–2200 h^{-1}. On the contrary, the mono-*tert*-butyl-substituted **Ni1** and the unsubstituted **Ni6** were not active under the same conditions, confirming that the absence of *ortho*-aryl substituents or monosubstitution in *ortho*-aryl positions is not efficient in protecting active centers from chain-transfer.[20,46] Under these conditions, a correlation exists between the activity, the ligand sterics, and the monomer length (Figure 2). Specifically, the TOF increases with decreasing the bulk of the *ortho*-substituents (Figure 2). For disubstituted complexes, TOF increases in the following order **Ni2** < **Ni3** < **Ni4**. A similar trend in TOF was observed by Chen and co-workers for the polymerization of 1-hexene with α-diimine Pd(II) complexes.[61]

Consistent with the trend of TOF, the molecular weight of the resulting polymers increase with decreasing the bulk of the *ortho*-substituents. Additionally, we found that **Ni5**, with a methyl group on the *para*-aryl position, was considerably more active than its *para*-hydrogen **Ni4** counterpart. This suggests that the presence of an electron-donating methyl group in the *para*-position has a positive effect on the activity.[46] Likewise, the introduction of methyl group in *para*-position led to an increase in polymer molecular weight. These effects can be ascribed to the perturbation of the metal electronics and steric environment on the nickel center, as also revealed by the molecular structure of **Ni5** (Figure 1). In other words, the

Table 1. Polymerization of 1-Octene, 1-Decene, and 1-Octadecene Using Ni1−Ni6 and a Reaction Time of 10 min[a]

entry	complex	yield (mg)	conv (%)	TOF[b] (h^{-1})	M_n[c] ($\times 10^3$)	M_w/M_n[c]	N[d]
1-octene							
1	**Ni1**	–					
2	**Ni2**	58	3	304	14.9	1.5	0.39
3	**Ni3**	187	10	980	37.4	1.2	0.50
4	**Ni4**	308	17	1614	52.8	1.3	0.58
5	**Ni5**	424	24	2220	57.9	1.2	0.73
6	**Ni6**	–					
1-decene							
7	**Ni1**	–					
8	**Ni2**	66	3	277	26.7	1.2	0.25
9	**Ni3**	197	9	826	50.5	1.2	0.39
10	**Ni4**	356	16	1493	56.0	1.3	0.64
11	**Ni5**	421	19	1766	59.0	1.4	0.71
12	**Ni6**	–					
1-octadecene							
13	**Ni1**	–					
14	**Ni2**	50	1	213	31.8	1.4	0.16
15	**Ni3**	80	2	342	55.8	1.4	0.14
16	**Ni4**	417	10	972	66.4	1.3	0.63
17	**Ni5**	534	13	1244	73.8	1.3	0.72
18	**Ni6**	–					

[a]Polymerization conditions: toluene, total volume, 16 mL; Ni, 10 μmol; Al/Ni molar ratio, 200; temperature, 22 °C; monomer concentration, 1.0 mol/L; time, 10 min. [b]Turnover frequency (TOF), calculated by the equation $mol_{pol}/(mol_{Ni} \times h)$. [c]Molecular weight ($M_n$) and molecular weight distribution (M_w/M_n) from SEC. [d]N = polymer yield/($mol_{Ni} \times M_n$).

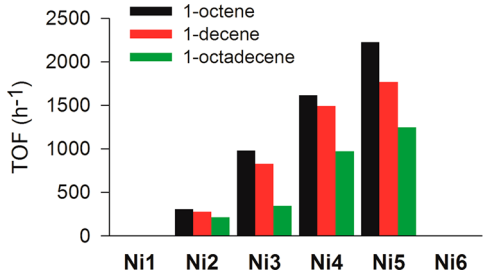

Figure 2. TOF vs the nickel complex employed.

positive effect of the presence of the electron-donating methyl groups in the *para*-position is due to the stabilization of the electron-deficient and coordinatively unsaturated active intermediate.[47,62−64] In agreement with the above results, the efficiency of each catalyst expressed by the number of polymer molecules produced per molecule of complex (N in Table 1) increases in the same order of TOF. The N values are lower than one, suggesting an incomplete activation for all the catalysts; however, increased initiation efficiency was found for **Ni4** and **Ni5**.

On the other hand, the TOF decreases with increasing the monomer length likely due to steric reasons (Figure 2). By increasing the monomer size, the steric hindrance of the growing polymer chain increases, thus retarding the new monomer insertion and limiting the chain propagation rate.

We also carried out the same experiments at longer polymerization times in order to collect enough material to make a thorough characterization. However, shorter polymerization times were chosen for less bulky and more active complexes (i.e., **Ni3−Ni5**) and 1-octadecene to limit changes in mixing of the solution when running polymerization at this scale.[65] The results are summarized in Table 2.

The polymers have molecular weights in the range from 68.5 to 159.6 × 10^3 g/mol. The molecular weight distributions increase slightly with respect to the experiments at short reaction time (Table 1) but still remain below 2. The fact that M_w/M_ns remain below 2 implies that M_n data are not yet limited by chain termination, and longer polymerization time would afford higher molecular weight polymers.[53] Under these conditions, the polymers molecular weight increases moving from **Ni1** to **Ni3** and then decreases for **Ni4** and **Ni5**. This result could be partly explained by the difference of the initiation efficiency for individual complexes. Moreover, the large amount of polymer formed with **Ni4** and **Ni5** (which exhibit the higher initiation efficiency) with consequent increase of the solution viscosity, and hence embedment of the active nickel species, may also contribute to the observed data limiting monomer diffusion and chain propagation.

The total branching level was calculated by ^{1}H NMR (Table 2). All the obtained polymers are less branched than would correspond to a regular and exclusive 1,2-enchainment, i.e., 125 branches/1000C for poly(1-octene), 100 branches/1000C for poly(1-decene), and 56 branches/1000C for poly(1-octadecene). This is because nickel walks along the growing polymer chain, rendering branches of various lengths (Scheme 1, path A) and long methylene units through the ω,1-enchainment (Scheme 1, path B1). The overall trend is that the fraction of ω,1-enchainment ranges from 46 to 62%, thus confirming that this class of complexes exhibits regiorandom insertion of α-olefins; i.e., they do not have a significant selectivity for 1,2- vs 2,1-insertion (Table 2).[21,29] Generally, **Ni1** gives less branched polymers with the highest degree of ω,1-rearrangement (lowest % of 1,2-insertion). Energetically less favorable, 2,1-insertion is more favored for **Ni1**. This is because before a 2,1-insertion the alignment between the C═C double bond of the monomer and the Ni−alkyl bond results in an interaction of the monomer chain with an *ortho* hydrogen atom, thus giving transition states that are less sterically congested than in the case in which both the *ortho* positions are substituted.[34,52] For the disubstituted complexes **Ni2−Ni4**, reducing the steric bulk of the ligand from the *ortho*-isopropyl to *ortho*-methyl groups resulted in a more branched polymer, although the differences became less pronounced with increasing the monomer size (Table 2). In the case of 1-octadecene, the branching level of the resulting polymers ranged from 23 to 32/1000C, narrower than that usually found for the polymers obtained using ethylene as the feedstock.[20,37] Chen and co-workers found the same trend in the case of 1-hexene and attributed this results to the low coordination capability of 1-hexene and, in general, to the difficulty for α-olefins to trap the secondary metal−alkyl species.[61]

The polymers were further characterized by ^{13}C NMR for quantification of individual branch levels.[56] The results are summarized in Table 3. The polymers made with **Ni2−Ni5** show two major branch lengths. The most abundant branches are methyl and longer than butyl branches (Lg): typical signals of methyl ($1B_1$ at 17.86 ppm) and longer branches ($1B_n$ at 12.01 ppm and $2B_n$ at 20.68 ppm) are safely identified in the ^{13}C NMR spectra (Figure 3C−E). Only very weak signals of carbons of ethyl, propyl, and butyl branches are detected.

Conversely, 1-octene and 1-decene polymers generated with **Ni1** result in more rearranged structures. The ^{13}C NMR spectra

Table 2. Polymerization of 1-Octene, 1-Decene, and 1-Octadecene Using Ni1−Ni5[a]

entry	complex	time (h)	yield (g)	conv (%)	M_n[b] (×10^3)	M_w/M_n[b]	branches/1000C[c]	ω,1[c] (%)
	1-octene							
19	**Ni1**	5	0.2	12	79.3	1.5	53	62
20	**Ni2**	3	1.1	62	105.6	1.3	66	53
21	**Ni3**	3	1.5	82	124.4	1.6	70	51
22	**Ni4**	3	1.7	94	118.3	1.7	75	48
23	**Ni5**	3	1.8	100	101.1	1.8	73	49
	1-decene							
24	**Ni1**	22	0.2	8	68.5	1.7	49	55
25	**Ni2**	3	1.0	43	115.3	1.4	55	53
26	**Ni3**	3	1.8	80	159.6	1.7	58	48
27	**Ni4**	3	2.2	98	128.1	1.7	61	46
28	**Ni5**	2	2.2	99	120.1	1.7	61	46
	1-octadecene							
29	**Ni1**	485	0.2	5	105.5	1.8	23	60
30	**Ni2**	3	0.5	13	134.7	1.5	25	57
31	**Ni3**	1	1.1	27	152.5	1.3	31	47
32	**Ni4**	1	1.7	43	146.2	1.6	32	49
33	**Ni5**	1	2.5	62	117.9	1.8	31	47

[a]Polymerization conditions: toluene, total volume, 16 mL; Ni, 10 μmol; Al/Ni molar ratio, 200; temperature, 22 °C; monomer concentration, 1.0 mol/L. [b]Molecular weight (M_n) and molecular weight distribution (M_w/M_n) from SEC. [c]From ^{1}H NMR. The term ω,1 implies that an olefin has inserted and then chain-walked to give an insertion that is through the ω and 1 carbon atoms. **Ni6** is not active.

Table 3. Microstructural Data and Thermal Properties

		CH_3/1000C[b]								
entry	total[a] CH_3	Me (%)	Et (%)	Pr (%)	Bu (%)	Lg (%)	T_g[c] (°C)	T_m[c] (°C)	ΔH_m[c] (J/g)	X_{DSC}[c] (%)
	1-octene									
19	53	26 (49)	2 (3)	1 (2)	0.4 (1)	24 (45)	−41	63	60	21
20	60	27 (45)				32 (53)	−47	49	34	12
21	68	30 (44)				37 (55)	−49	37	23	8
22	68	31 (45)				36 (53)	−50	36	22	8
23	69	33 (48)				35 (51)	−49	38	23	8
	1-decene									
24	51	20 (39)	4 (8)	2 (4)	1 (2)	24 (47)	−43	72	55	19
25	52	21 (40)				30 (58)	−46	54	40	14
26	59	22 (37)				36 (61)	−46	48	31	10
27	62	27 (43)				34 (55)	−46	47	31	10
28	60	24 (40)				35 (58)	−47	47	30	10
	1-octadecene									
29	26	11 (42)				15 (58)		96	113	39
30	30	11 (37)				19 (63)		85	97	33
31	35	9 (26)				26 (74)		65	78	27
32	36	10 (28)				26 (72)		63	73	25
33	34	9 (26)				25 (74)		64	74	25

[a]Total methyls by ^{13}C NMR. [b]Distribution of the main branch levels by ^{13}C NMR. [c]From DSC (second heating, T_m at peak maximum).

clearly show signals due to carbons of ethyl ($1B_2$ at 9.0 ppm), propyl ($1B_3$ at 12.51, $2B_3$ at 18.08 ppm and $3B_3$ at 34.66 ppm), and butyl branches ($2B_4$ at 21.1 ppm) (Figure 3B).[54] Although these signals are small in comparison to the others, their presence indicates that insertion paths, different from those shown in Scheme 1, become more competitive. The presence of these branches reflects a significant extent of chain-walking and the high propensity of **Ni1** to promote 2,1-insertion. Indeed, ethyl, propyl, and butyl branches are the result of 2,1-insertion followed by repetitive and sequential β-hydride elimination, alkene rotation, and readditions (with opposite regiochemistry) that relocates the active nickel center along the growing polymer chain (Scheme 2, path B2).[66] We found that 1-octene polymer includes a 3% of ethyl branch, 2% of propyl branch, and 1% of butyl branch, while the 1-decene polymer includes a 8% of ethyl branch, 4% of propyl branch, and 2% of butyl branch (Table 3). These results indicate that the intermediate B2/6 in Scheme 2, formed when the metal is at C6 position (C8 for 1-decene), which installs an ethyl branch in the polymer chain, is stable enough (and most favored) to allow further monomer insertion, followed by the intermediate B2/5 formed when the metal is at C5 (which installs a propyl branch; C7 for 1-decene) and B2/4 formed when the metal is at C4 (which installs a butyl branch; C6 for 1-decene). Also of note, the presence of ethyl, propyl, and butyl branches indicates that a part of methyl branches in these polymers from **Ni1** could be formed also through a 2,1-enchainment followed by successive β−H elimination and reinsertions (path B2) that

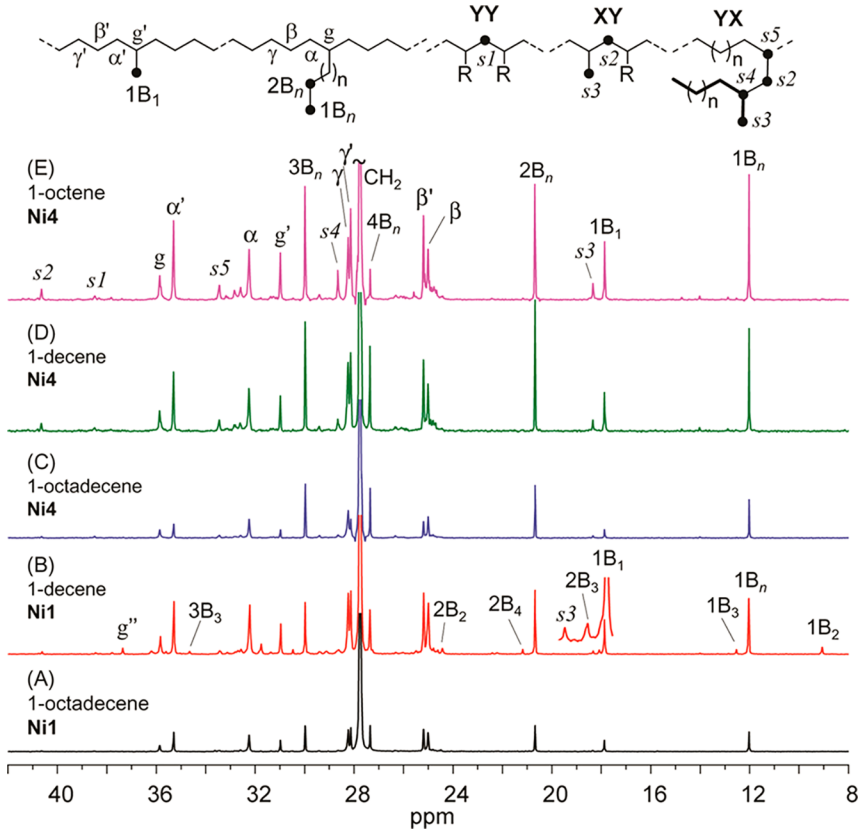

Figure 3. ^{13}C NMR spectra of (A) entry 29, (B) entry 24, (C) entry 32, (D) entry 27, and (E) entry 22. R is a branch longer than butyl. Refer to Scheme 2 for signals ascribed to butyl ($2B_4$), propyl ($1B_3$, $2B_3$ and $3B_3$), and ethyl isolated branches ($1B_2$, $2B_2$, and g″, see Scheme 2).

Scheme 2. Mechanism for the Formation of Butyl, Propyl, and Ethyl Branch (*β*-H elim + *ins* = *β*-H Elimination and Insertion; *ins* = Monomer Insertion) for 1-Octene Polymerization (g″ at 37.4 ppm)

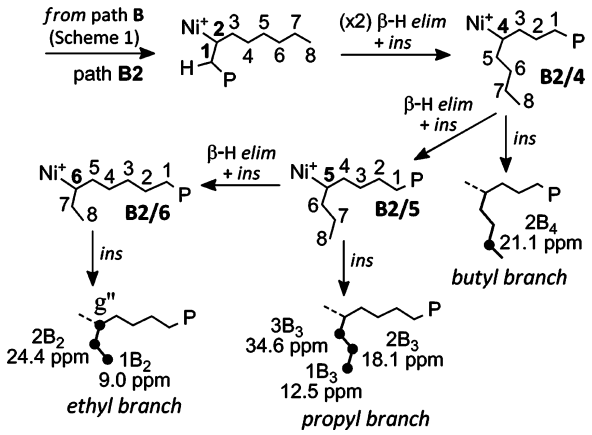

relocates the nickel at C7 position (C9 for 1-decene). However, it is impossible to distinguish a methyl branch generated from paths B2 and A1 since they both result in the same branching defect.

On the other hand, the 1-octadecene sample generated with **Ni1** show only methyl and long branches (Figure 3a). This suggests that insertion of 1-octadecene into a secondary Ni–alkyl bond do not occur with **Ni1** and that the metal prefers to migrate to ω carbon: the 2,1-insertion of 1-octadecene preferentially evolves into a 18,1-enchainment to give long methylene sequences (Scheme 1, path B1).

The length of the monomer significantly affects the branch-type distribution, long branches being increasingly predominant as the α-olefin size increases (Table 3). The higher percentage of longer than butyl branches with respect to methyl branches indicates that after a 1,2-insertion a further 1,2 insertion without chain-walking is favored (Scheme 1, path A2). The amount of ω,2-enchainment, that is 1,2-insertion followed by chain-walking, which installs a methyl in the polymer chain (Scheme 1, path A1) decreases in favor of 1,2-enchainment (which installs a long branch) with increasing the monomer size. This is likely due to the fact that the probability of migration up to the terminal ω carbon of the last-inserted monomer unit (which is much more space demanding than 1,2-enchainment) decreases for longer α-olefins.[25]

On the whole, chain-walking occurs more frequently in the polymerization of α-olefins catalyzed by **Ni1** and the formation of ethyl, propyl, and butyl branches also indicates that insertion into a secondary Ni–alkyl bond, particularly for 1-octene and 1-decene, occurs. Therefore, the fact that **Ni1** spends more time walking along the polymer chain, rendering linear PE-like units (much more favorable ω,1-enchainment) and alkyl branching of different lengths may contribute also to its low turnover rate, which in turn limits the molecular weight of the polymers that can be achieved (Table 2).[40]

Further information comes from ^{13}C NMR spectrum (Figure 3). All the polymers show weak signals at 38.4 and 40.6 ppm ascribed to α,α-methylene carbons ($s1$ and $s2$, respectively) and at 18.3 ppm ascribed to a methyl carbon ($s3$ of structure **YX**, Figure 3).[67] According to previous assignment,[34] $s1$ at 38.4 ppm corresponds to the α,α-methylene carbon of the structure **YY**–CH(R)CH$_2$CH(R)– (R > butyl), while $s2$ at 40.6 ppm to

the α,α-methylene carbon of the structure **XY**−CH(R)CH_2CH(Me)− (R > butyl). We can relate these signals to the mechanistic pathways. Indeed, on the basis of the chain-walking coordination/insertion mechanism model, the structure **YY** comes from two successive 1,2-insertions without chain-walking (Scheme 3, path C1a), while structures **XY** and

Scheme 3. Modes of Monomer Enchainment before the Last 1,2-Inserted Unit (CW = Chain-Walking; *ins* = New Further Insertion; 1,2-ench = 1,2-Enchainment)

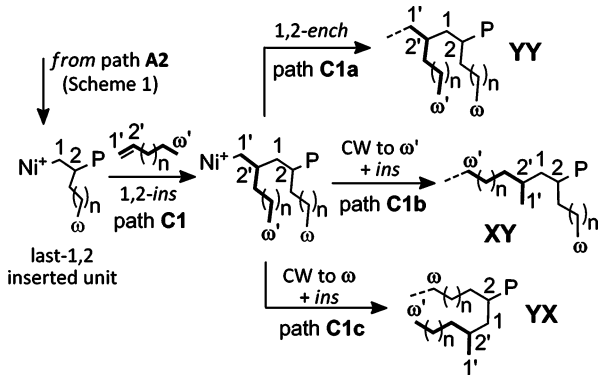

YX come from a 1,2-insertion on the last 1,2-enchained unit followed by chain-walking: **XY** if nickel gives chain-walking to ω' (Scheme 3, path C1b), **YX** if nickel gives chain-walking to ω (Scheme 3, path C1c). As a result, ^{13}C NMR can be used to calculate the relative amount of structure **YY** and **XY**+**YX** (by ^{13}C NMR it is not possible to differentiate between **XY** and **YX** structures[34]). The results are summarized in Table 4. As mentioned above, the regiochemistry of monomer insertion is

Table 4. Ligand Effect on the Insertion Paths after the Last 1,2-Inserted Unit

		2,1-ins[a]	1,2-ins[b]		
entry	complex	(%)	YY[c] (%)	XY + YX[d] (%)	YY/(XY + YX)
1-octene					
19	**Ni1**	89.8	4.1	6.1	0.67
20	**Ni2**	81.1	8.0	12.0	0.67
21	**Ni3**	81.9	8.6	9.5	0.90
22	**Ni4**	79.2	10.1	10.7	0.94
23	**Ni5**	79.9	10.1	10.0	1.02
1-decene					
24	**Ni1**	94.6	2.4	2.9	0.83
25	**Ni2**	81.9	8.4	9.7	0.87
26	**Ni3**	78.9	10.3	10.8	0.95
27	**Ni4**	78.7	10.4	10.8	0.96
28	**Ni5**	80.9	9.6	9.5	1.01
1-octadecene					
29	**Ni1**	94.7	2.6	2.7	0.98
30	**Ni2**	82.1	9.0	8.9	1.01
31	**Ni3**	83.1	11.0	5.9	1.86
32	**Ni4**	83.0	11.1	5.9	1.90
33	**Ni5**	85.2	10.2	4.6	2.22

[a]A 2,1-insertion, after that a 1,2-enchained unit is installed in the polymer backbone. [b]A 1,2-insertion, after that a 1,2-enchained unit is installed in the polymer backbone. [c]Structure **YY** generated from path C1a (Scheme 3). [d]Structures **XY** and **YX**, generated from paths C1b and C1c, respectively (Scheme 3). **XY** and **YX** are not distinguishable from ^{13}C NMR.

mostly random: after the last 1,2-inserted unit, there is a large amount of 2,1-insertion (associated with path B in Scheme 1 and Table 4).

For **Ni1**, 2,1-insertion on the last 1,2-inserted unit account for 90% and more, while for **Ni2**−**Ni5** path B slightly decreases in favor of more competing path C1 associated with two consecutive 1,2-insertions (Scheme 3). The type of ligand as well as the length of the monomer has a great effect on path C1. In the case of 1-octene, the formation of **XY** + **YX** structures, associated with path C1b/c, is favorable with **Ni1** and **Ni2**, while for **Ni3**−**Ni5** the frequency of paths C1a and C1b/c is the same. The ligand substitution does not play a key role in the shift of insertion mode for 1-decene, the formation of structure **YY** and **XY** + **YX** being equally probable for all the investigated complexes. Finally, unlike with 1-octene, in the case of 1-octadecene, the two paths have almost the same chance of happening with **Ni1** and **Ni2**, while structure **YY**, associated with path C1a, seems to be sound for **Ni3**−**Ni5**. The highest **YY**/(**XY** + **YX**) ratio was found for **Ni5**, for which the probability that 1,2-insertion on the last 1,2-enchained unit undergoes a successive insertion (1,2-enchainment, path C1a) is more than twice the probability that 1,2-insertion on the last 1,2-enchained unit undergoes chain-walking before the new insertion (Table 4, entry 33).

Changes in the branching density and distribution affect the thermal properties of the polymers. The thermal behavior of the polymers was investigated by DSC, and the results are reported in Table 3. Figure 4A shows the thermograms of the polymers synthesized with **Ni2**. Glass transition events at low temperature and broad melting endotherms can be observed. Generally, the glass transition temperature (T_g), the melting peak temperature (T_m), and the melting enthalpy (ΔH_m) of the polymers increase with increasing the monomer length. Despite comparable ω,1 fraction (Table 2), the length of linear segments increases with the monomer chain length, resulting in higher melting points.

Figure 4B compares the thermograms of all the 1-decene polymers. The polymer from **Ni1** (Table 3, entry 24) exhibits the highest T_m (72 °C) and crystallinity (19%). Among the other investigated complexes, **Ni2** bearing bulky isopropyl groups gives the polymer with the highest T_m (54 °C) and crystallinity (14%). DSC analysis of 1-decene polymers by less bulky complexes, i.e., **Ni3**−**Ni5**, shows comparable broad endotherms with similar melting point and enthalpy.

A similar trend of melting behavior as a function of nickel complex was observed for 1-octene and 1-octadecene polymers. The thermal data are strictly related to the polymer microstructure, T_m and ΔH_m increasing with the increase of crystallizable methylene sequences generated from the ω,1-enchainment. Figure 4C plots ΔH_m versus the number of branches longer than methyl. A relationship between the two data was found and enhancing the content of longer than methyl side groups the melting enthalpy decreases. An analogous trend was observed for T_m.

The synthesized polymers were structurally characterized by X-ray techniques. WAXD patterns of 1-octene and 1-decene polymers obtained with **Ni2**−**Ni5** show a diffuse peak centered at about 20 2θ°, while the patterns of the polymers from **Ni1** show a weak peak at about 21.5 2θ° followed by a broad shoulder, thus confirming an increase in the crystalline content (Figure 5A). The WAXD data together with the low T_ms and broad melting range suggest the existence of a fringed-micellar

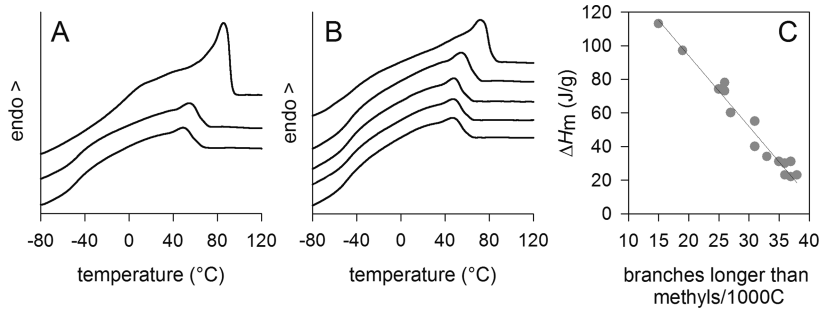

Figure 4. DSC traces of (A) 1-octene, 1-decene, and 1-octadecene polymer from **Ni2** (entries 20, 25, and 30, from top to bottom) and (B) 1-decene polymers obtained from **Ni1**–**Ni5** (entries 24–28 from top to bottom). (C) Plot of melting enthalpy (ΔH_m) as a function of the total branching longer than methyl. The line is a guide to the eye and illustrates the overall trend.

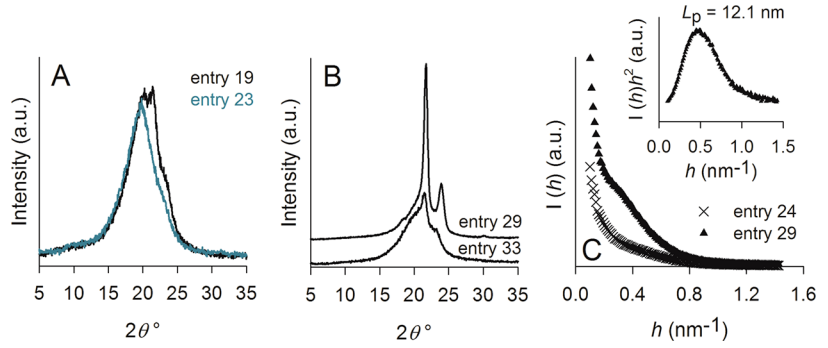

Figure 5. WAXD profiles of (A) 1-octene polymers from **Ni1** and **Ni5** (entries 19 and 23) and (B) 1-octadecene polymers from **Ni1** and **Ni5** (entries 29 and 33). (C) SAXS profile of 1-decene and 1-octadecene polymers from **Ni1** (entries 24 and 29). In the inset, the Lorentz correct scattering intensity of entry 29 is shown.

Table 5. Mechanical Properties

entry	E^a (MPa)	σ^a (MPa)	ε^a (%)	SR_I[b]	SR_X[c]	$SR_{550\%}$[d]	$SR_{1200\%}$[e]
1-octene							
20	5.8 ± 0.7	10.6 ± 1.0	1420 ± 90	65	54	63	59
21	2.1 ± 0.4	5.4 ± 0.6[f]	>1900[g]	79	67	76	71
22	1.9 ± 0.4	3.6 ± 0.5[f]	>1900[g]	80	66	75	68
23	2.1 ± 0.3	2.8 ± 0.3[f]	>1900[g]	75	61	71	63
1-decene							
25	7.5 ± 0.3	15.5 ± 0.4	1388 ± 29	59	47	56	53
26	4.1 ± 0.5	10.6 ± 1.6	1397 ± 87	67	54	65	63
27	3.8 ± 0.9	9.6 ± 1.0	1503 ± 65	64	50	61	59
28	3.6 ± 0.4	9.0 ± 1.2	1476 ± 77	62	48	60	57
1-octadecene							
30	48.7 ± 1.5	22.9 ± 1.0	670 ± 48	27	16	16	n.d.[h]
31	38.4 ± 1.9	17.4 ± 1.4	638 ± 72	20	12	14	n.d.[h]
32	32.1 ± 2.0	20.7 ± 1.3	774 ± 69	23	13	15	n.d.[h]
33	30.5 ± 2.2	20.4 ± 1.6	799 ± 50	22	13	16	n.d.[h]

[a]Young's modulus (E), ultimate tensile strength (σ), and elongation at break (ε). [b]Strain recovery measured after the first step in a step cycle test type at 300% strain. [c]Strain recovery measured after the last step in a step cycle test type at 300% strain. [d]Strain recovery measured after the strain at 550% in a step cycle test type at increasing strains. [e]Strain recovery measured after the strain at 1200% in a step cycle test type at increasing strains. [f]Stress at 1900% [g]Instrument detection limit. [h]The specimens break before the strain at 1200% in a step cycle test type at increasing strains.

crystal structure with a broad size distribution that comes from the statistical distribution of crystallizable chain lengths.[68,69]

WAXD diffractograms of 1-octadecene polymers show the typical diffractions of poly(ethylene) orthorhombic crystalline structure: sharp patterns were collected for entries 29 and 30 (from **Ni1**–**Ni2**) while the profiles result less definite for entries 31, 32, and 33 (from **Ni3**–**Ni5**) characterized by lower crystallinity degree (Figure 5B).

The polymers supermolecular structure was further investigated by SAXS. The 1-octene and 1-decene polymers showed low-intensity scattering profiles, similar to those of 1-octene copolymers with low crystallinity previously reported.[22] The scattering profile of 1-octadecene polymers shows a discrete peak which is associated with the long period (L_p) that results from the electron density difference between crystalline and amorphous phases (Figure 5C). The structural data together with the crystallinity and the melting temperature of the 1-

octadecene polymers are consistent with a mixed morphology containing both bundled crystals and lamellar structures.[70,71]

Mechanical Properties. First investigation on the mechanical behavior of 1-octene, 1-decene, and 1-octadecene polymers obtained with **Ni2**–**Ni5** was carried out at 20 °C by uniaxial stretching until failure. The tensile properties are summarized in Table 5, and selected stress–strain curves are shown in Figure 6. Figure 6A shows the tensile strength curves

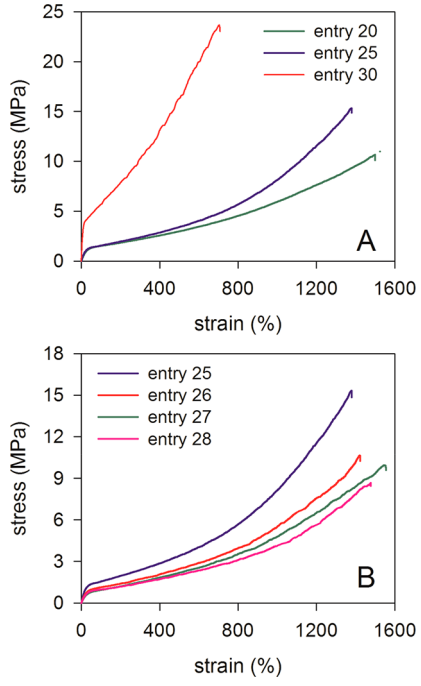

Figure 6. Stress–strain curves of (A) 1-octene, 1-decene, and 1-octadecene from **Ni2** (entries 20, 25, and 30) during monotonic tensile deformation and (B) 1-decene polymers from **Ni2**–**Ni5** (entries 25–28) during monotonic tensile deformation.

of the polymers obtained with **Ni2**. 1-Octene and 1-decene polymers show stress–strain curves with typical features of elastomers, i.e., low modulus and high elongation at break. Compared to these polymers, 1-octadecene polymer exhibits different tensile behavior due to longer crystallizable methylene sequences in the polymer backbone, with higher modulus and ultimate strength, but lower elongation at break. The stress–strain curve of 1-octadecene polymer exhibits more evident yielding phenomena and a steady increase of the stress (Figure 6A).

Figure 6B compares the tensile strength curves of 1-decene polymers generated using **Ni2**–**Ni5**. The strain deformation of the more crystalline polymer from **Ni2** (Table 5, entry 25) proceeds with the highest Young's modulus (7.5 MPa) and stress at break (15 MPa). 1-Decene polymers from **Ni3**–**Ni5**, which have similar crystallinity, exhibit comparable tensile behavior with a Young's modulus of about 4 MPa and ultimate tensile strength, in the range from 9.0 to 10.5 MPa.

All the 1-decene polymers showed high and similar ultimate strain (about 1450 ± 50%), regardless of crystallinity. A similar trend of Young's modulus as a function of the crystallinity was found for 1-octene polymers. However, it is worth emphasizing that the low crystallinity 1-octene polymers, i.e., entries 21–23, display impressive strain at break values approaching 2000%. The 1-octadecene polymers differ mainly in Young's modulus, which ranges from 49 to 30 MPa with decreasing the polymer crystallinity (from 33 to 25%, Table 3).

The elasticity of the polymers, i.e., the capability to return to the initial state once the force is removed, was evaluated from step cycle tensile tests. In the first set of experiments, the samples were subjected to ten repetitive stress–strain cycles with a maximum of 300% strain, and the elastic recovery in specimen length was measured after removal of the strain for each cycle. The first cycle results in the most significant amount of permanent deformation, followed by minimal increase in the unrecovered strain on subsequent cycles (Figure 7).

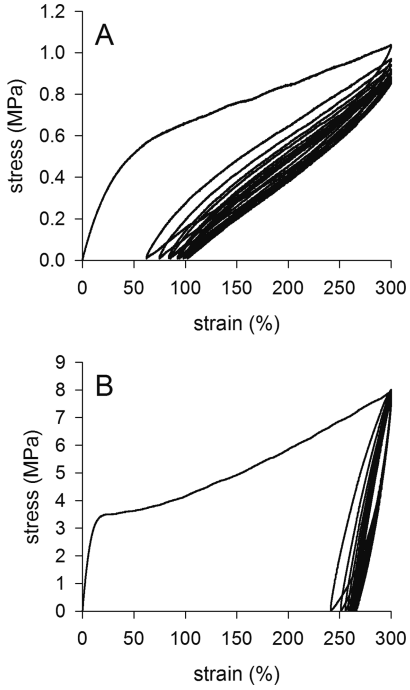

Figure 7. Stress–strain curve of (A) 1-octene polymer from **Ni3** (entry 21) and (B) 1-octadecene polymer from **Ni3** (entry 31) in the hysteresis experiment for ten cycles at 300% strain.

The main difference between the cyclic deformation behavior of the investigated polymers is in the amount of unrecovered strain after the first cycle. For 1-octene and 1-decene polymers the strain recovery after the first load cycle ranges from 59 to 80% and increases with decreasing the polymer crystallinity (SR_I in Table 5). The more amorphous poly(1-octene)s (Table 5, entries 21–23) display similar recovery over the whole cycle tensile test and the highest elastic recovery of about 67% after the last load cycle (SR_X in Table 5 and Figure 7A). In contrast, 1-octadecene polymers exhibit high amount of permanent deformation after the first cycle with SR_I values ranging from 20 to 27% and very low strain recovery (ca. 15%) after the last cycle (Figure 7B). These data indicate that the 1-octadecene polymers are not elastomers and permanently deform upon stretching.

In the second set of cyclic experiments, the samples were extended step by step up to different strains until fracture. As typical examples, the stress–strain curve during cyclic tensile deformation of 1-decene polymer (entry 26) and 1-octadecene polymer (entry 31) are shown in Figures 8A and 8B, respectively. Based on the curves, the strain recovery values were obtained (Table 5). Generally, the strain recovery decreases rapidly at lower applied strains and then tends to

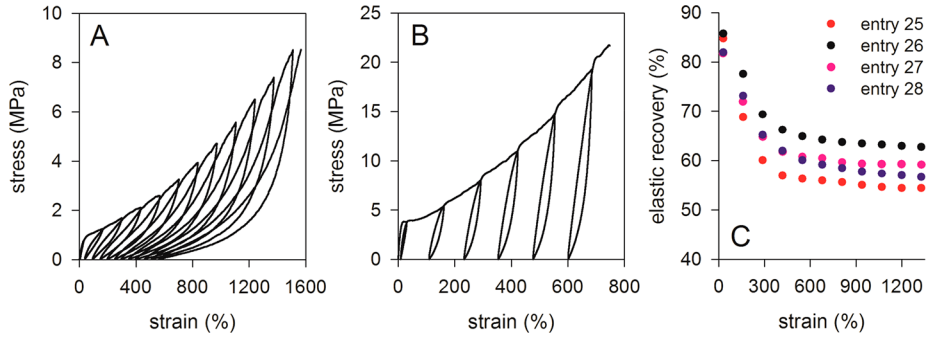

Figure 8. Stress–strain curve of (A) 1-decene polymer from Ni3 (entry 26) and (B) 1-octadecene polymer from **Ni3** (entry 31) during step cycle tensile deformation at different strain. (C) strain recovery as a function of the applied strain for 1-decene polymers from **Ni2**–**Ni5** (entries 25–28).

level off at higher applied strains. As a typical example, the strain recovery as a function of the applied strain for 1-decene polymers is reported in Figure 8C. 1-Octene and 1-decene polymers exhibit similar behavior with comparable and high SR values for the whole range of applied strains ($SR_{550\%}$ and $SR_{1200\%}$ in Table 4), whereas the 1-octadecene polymers present very low recovery of 15% when the strain was equal to 550%.

As a further experiment, the 1-octene and 1-decene thermoplastic elastomers were subjected to creep test in order to evaluate their resistance to permanent deformation. Samples were elongated to 300% strain and held at a constant stress for 3 h. It is worth pointing out that every sample required typical stress value in order to achieve 300% strain (from 1.2 MPa for the low crystallinity 1-octene polymers to 2.8 MPa for the highest crystallinity 1-decene polymer). Selected strain–time curves are shown in Figure 9. The low crystallinity 1-octene and 1-decene polymers exhibited great deformation over time, particularly those generated with **Ni3**–**Ni5**.

Overall, the obtained polymers exhibited a broad spectrum of tensile properties, strongly depending on the crystallinity, that is, the monomer length and the type of α-diimine ligand. The tensile tests show that 1-octene and 1-decene polymers behaved as elastomers with properties close to those reported for TPEs of random ethylene/α-olefin copolymers.[32,72,73] These materials retain excellent mechanical properties, i.e., high elongation at break and good strain recovery, even after being melted and reprocessed several times (Figure S14). Conversely, 1-octadecene polymers behaved as plastomers, exhibiting properties intermediate between those of an elastomer and a LLDPE-like material.[70,74]

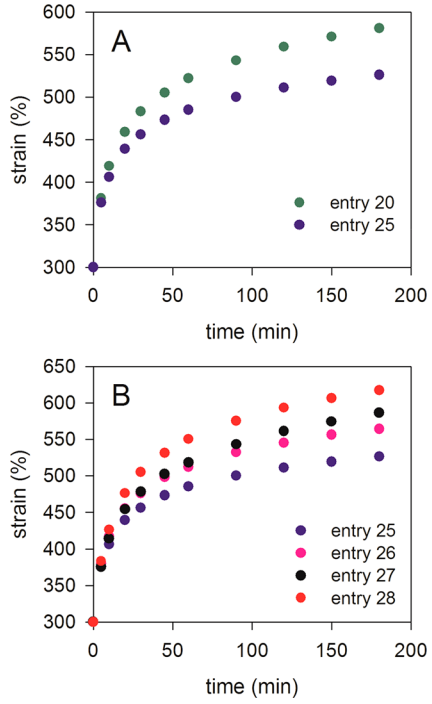

Figure 9. Creep experiments of (A) 1-octene and 1-decene from **Ni2** (entries 20 and 25) and (B) 1-decene polymers from **Ni2**–**Ni5** (entries 25–28).

CONCLUSIONS

We report for the first time a systematic investigation on the polymerization of 1-octene, 1-decene, and 1-octadecene catalyzed by a series of α-diimine Ni(II) complexes with methyl ligand backbone and different substituents in *ortho*- and *para*-aryl positions. In addition to the bulky isopropyl and *tert*-butyl substituents described in the Brookhart's works,[37,53] complexes with different aryl *ortho*- and *para*-substituted α-diimine ligands, including the less sterically demanding methyl and ethyl substituents are investigated (**Ni1**–**Ni6**). The crystal structures of **Ni3**–**Ni6** are reported. Interestingly, despite their relative structural similarity, all species crystallized in different space groups, suggesting that beside their different catalytic properties, which is the focus of this work, their differential substitution is also likely to guide and affect the packing arrangement of these species in the solid state.

We demonstrate that for the polymerization of higher α-olefins two methyl substituents on the *ortho*-positions of the α-diimine ligand are bulky enough to exhibit a certain steric effect, retarding the free rotation of aniline moieties and hence decreasing the β–H elimination and subsequent chain transfer. This feature allows the synthesis of high molecular weight polymers and more branched than those obtained with bulky isopropyl and *tert*-butyl substituents, while maintaining high turnover frequencies. In addition, **Ni5**, with two methyl groups on the *ortho*-positions and a methyl on the *para*-position, was more active than its *para*-H **Ni4** complex, suggesting that the presence of the methyl in the *para* position has a further positive effect on the turnovers/h due to the stabilization of the reactive, electron-deficient, and coordinatively unsaturated alkyl agostic intermediate. Moreover, it is pointed out that at short polymerization time, i.e., assuming no complications due to mass transfer limitations and insufficient mixing, modifying the *ortho* substituents from methyl to isopropyl groups, the

complexes bearing less bulky methyl groups afford higher molecular weight polymers at significantly higher turnovers/h.

The polymers were characterized by ^{13}C NMR for quantification of the total branching level and branch-type distribution. Subtle changes in the α-diimine ligand structure and monomer size have important effects on the numerous combinations of monomer insertion and chain-walking paths from which different branches are installed. The thermal properties and crystallinity of the polymers vary depending on the extent of branching and the branch-type distribution. Generally, polymers from 1-octene and 1-decene exhibit low melting temperatures and a broad melting range likely due to the fringed-micellar crystal structure with a broad size distribution, while the structural data and melting behavior of 1-octadecene polymers suggest the presence of a mixed morphology containing both bundled crystals and lamellar structures. Accordingly, the tensile tests show that the 1-octene and 1-decene polymers behave as elastomers exhibiting low modulus, high elongation at break, and good elastic recovery, while 1-octadecene polymers show evident yielding phenomena and plastic deformation.

To conclude, this work provides new insights into the polymerization of long chain α-olefins catalyzed by α-diimine Ni(II) complexes with methyl ligand backbone and different alkyl substituents in *ortho*- and *para*-aryl positions. These systems prove great prospect due to the low cost and accessibility of starting reagents and monomer feedstocks and the high turnovers/h together with the reusability of the resulting polymers that retain excellent mechanical properties even after being melted and reprocessed several times.

ASSOCIATED CONTENT

Supporting Information

The Supporting Information is available free of charge on the ACS Publications website at DOI: 10.1021/acs.macromol.7b02242.

Experimental procedures, sample data, including ^{13}C NMR spectra, DSC traces, WAXD and SAXS patterns, and mechanical properties of all the polymers (PDF)

Single-crystal X-ray crystallographic data and spectral data for compound **Ni3** (PDF)

Single-crystal X-ray crystallographic data and spectral data for compound **Ni4** (PDF)

Single-crystal X-ray crystallographic data and spectral data for compound **Ni5** (PDF)

Single-crystal X-ray crystallographic data and spectral data for compound **Ni6** (PDF)

Accession Codes

CCDC 1566127−1566130 contain the crystallographic coordinates of the four structures described in this paper. These data can be obtained free of charge via www.ccdc.cam.ac.uk/data_request/cif.

AUTHOR INFORMATION

Corresponding Authors

*E-mail: fabio.bertini@ismac.cnr.it (F.B.).

*E-mail: giuseppe.leone@ismac.cnr.it (G.L.).

ORCID

Javier Martí-Rujas: 0000-0001-8423-2439

Giovanni Ricci: 0000-0001-8586-9829

Giuseppe Leone: 0000-0001-6977-2920

Present Address

J.M.-R.: Universitat Autònoma de Barcelona, Facultat de Ciències, Departament de Geologia, Campus de la UAB, Bellaterra, Catalonia, Spain.

Notes

The authors declare no competing financial interest.

ACKNOWLEDGMENTS

Financial support from MIUR (Ministero dell'Istruzione, dell'Università e della Ricerca) project PON-DIATEME 2007-2013. The authors thank Adriana Cacciamani, Fulvia Greco, and Daniele Piovani for skilled technical assistance.

REFERENCES

(1) Small, B. L.; Brookhart, M. Iron-Based Catalysts with Exceptionally High Activities and Selectivities for Oligomerization of Ethylene to Linear α-Olefins. *J. Am. Chem. Soc.* **1998**, *120*, 7143−7144.

(2) Dry, M. E. The Fischer−Tropsch process: 1950−2000. *Catal. Today* **2002**, *71*, 227−241.

(3) Inaba, M.; Murata, K.; Saito, M.; Takahara, I. Production of olefins from ethanol by Fe-supported zeolite catalysts. *Green Chem.* **2007**, *9*, 638−646.

(4) Stadler, F. J.; Piel, C.; Klimke, K.; Kaschta, J.; Parkinson, M.; Wilhelm, M.; Kaminsky, W.; Munstedt, H. Influence of Type and Content of Various Comonomers on Long-Chain Branching of Ethene/α-Olefin Copolymers. *Macromolecules* **2006**, *39*, 1474−1482.

(5) Chum, S.; Swogger, K. W. Olefin polymer technologies−History and recent progress at the Dow Chemical Company. *Prog. Polym. Sci.* **2008**, *33*, 797−819.

(6) Walton, K. L. Metallocene Catalyzed Ethylene/Alpha Olefin Copolymers Used in Thermoplastic Elastomers. *Rubber Chem. Technol.* **2004**, *77*, 552−568.

(7) Müller, G.; Rieger, B. Propene Based Thermoplastic Elastomers by Early and Late Transition Metal Catalysts. *Prog. Polym. Sci.* **2002**, *27*, 815−851.

(8) De Ballesteros, O. R.; De Rosa, C.; Auriemma, F.; Di Girolamo, R.; Scoti, M. Thermoplastic Elastomers from Binary Blends of Syndiotactic Polypropylenes with Different Stereoregularity. *Polymer* **2016**, *85*, 114−124.

(9) Moshonov, M.; Aharonovich, S.; Eisen, M. S. Tailor-Made Thermoplastic Elastomeric Stereoblock Polypropylenes by Modulation of Monomer Pressure. *Macromolecules* **2016**, *49*, 9287−9290.

(10) Crawford, K. E.; Sita, L. R. De Novo Design of a New Class of "Hard−Soft" Amorphous, Microphase-Separated, Polyolefin Block Copolymer Thermoplastic Elastomers. *ACS Macro Lett.* **2015**, *4*, 921−925.

(11) He, Z.; Liang, Y.; Yang, W.; Uchino, H.; Yu, J.; Sun, W.-H.; Han, C. C. Random Hyperbranched Linear Polyethylene: One Step Production of Thermoplastic Elastomer. *Polymer* **2015**, *56*, 119−122.

(12) Espinosa, E.; Charleux, B.; D'agosto, F.; Boisson, C.; Tripathy, R.; Faust, R.; Soulie-Ziakovic, C. Di- and Triblock Copolymers Based on Polyethylene and Polyisobutene Blocks. Toward New Thermoplastic Elastomers. *Macromolecules* **2013**, *46*, 3417−3424.

(13) Holden, G.; Kricheldorf, H. R.; Quirk, R. P. *Thermoplastic Elastomers*, 3rd ed.; Hanser Publishers: Munich, 2004.

(14) Drobny, J. G. *Handbook of Thermoplastic Elastomers*; William Andrews: New York, 2007.

(15) Deplace, F.; Scholz, A. K.; Fredrickson, G. H.; Kramer, E. J.; Shin, Y.-W.; Shimizu, F.; Zuo, F.; Rong, L.; Hsiao, B. S.; Coates, G. W. Tough and Elastic Thermoplastic Organogels and Elastomers Made of Semicrystalline Polyolefin-based Block Copolymers. *Macromolecules* **2012**, *45*, 5604−5618.

(16) De Rosa, C.; Auriemma, F.; Perretta, C. Structure and Properties of Elastomeric Polypropylene from C_2 and C_{2v}-Symmetric Zirconocenes. The Origin of Crystallinity and Elastic Properties in Poorly Isotactic Polypropylene. *Macromolecules* **2004**, *37*, 6843−6855.

(17) Hong, K.; Strobl, G. Network Stretching during Tensile Drawing of Polyethylene: A Study Using X-ray Scattering and Microscopy. *Macromolecules* **2006**, *39*, 268−273.
(18) Hiss, R.; Hobeika, S.; Lynn, C.; Strobl, G. Network Stretching, Slip Processes, and Fragmentation of Crystallites During Uniaxial Drawing of Polyethylene and Related Copolymers. A Comparative Study. *Macromolecules* **1999**, *32*, 4390−4403.
(19) Arriola, D. J.; Carnahan, E. M.; Hustad, P. D.; Kuhlman, R. L.; Wenzel, T. T. Catalytic Production of Olefin Block Copolymers via Chain Shuttling Polymerization. *Science* **2006**, *312*, 714−719.
(20) Ittel, S. D.; Johnson, L. K.; Brookhart, M. Late-Metal Catalysts for Ethylene Homo- and Copolymerization. *Chem. Rev.* **2000**, *100*, 1169−1204.
(21) Leone, G.; Mauri, M.; Pierro, I.; Ricci, G.; Canetti, M.; Bertini, F. Polyolefin Thermoplastic Elastomers from 1-Octene Chain-Walking Polymerization. *Polymer* **2016**, *100*, 37−44.
(22) Pierro, I.; Leone, G.; Zanchin, G.; Canetti, M.; Ricci, G.; Bertini, F. Polyolefin Thermoplastic Elastomers from 1-Octene Copolymerization with 1-Decene and Cyclopentene. *Eur. Polym. J.* **2017**, *93*, 200−211.
(23) Guo, L.; Dai, S.; Chen, C. Investigations of the Ligand Electronic Effects on α-Diimine Nickel(II) Catalyzed Ethylene Polymerization. *Polymers* **2016**, *8*, 37.
(24) Wang, F.; Tanaka, R.; Cai, Z.; Nakayama, Y. M.; Shiono, T. Synthesis of Highly Branched Polyolefins Using Phenyl Substituted α-Diimine Ni(II) Catalysts. *Polymers* **2016**, *8*, 160.
(25) Rose, J. M.; Cherian, A. E.; Coates, G. W. Living Polymerization of α-Olefins with an α-Diimine Ni(II) Catalyst: Formation of Well-Defined Ethylene−Propylene Copolymers Through Controlled Chain-Walking. *J. Am. Chem. Soc.* **2006**, *128*, 4186−4187.
(26) Wang, X.; Fan, L.; Ma, Y.; Guo, C.-Y.; Solan, G. A.; Sun, Y.; Sun, W.-H. Elastomeric Polyethylenes Accessible via Ethylene Homo-Polymerization Using an Unsymmetrical α-Diimino-Nickel Catalyst. *Polym. Chem.* **2017**, *8*, 2785−2795.
(27) Liu, J.; Chen, D.; Wu, H.; Xiao, Z.; Gao, H.; Zhu, F.; Wu, Q. Polymerization of α-Olefins Using a Camphyl α-Diimine Nickel Catalyst at Elevated Temperature. *Macromolecules* **2014**, *47*, 3325−3331.
(28) Killian, C. M.; Tempel, D. J.; Johnson, L. K.; Brookhart, M. Living Polymerization of α-Olefins Using Ni^{II}−α-Diimine Catalysts. Synthesis of New Block Polymers Based on α-Olefins. *J. Am. Chem. Soc.* **1996**, *118*, 11664−11665.
(29) Leone, G.; Mauri, M.; Bertini, F.; Canetti, M.; Piovani, D.; Ricci, G. Ni(II) α-Diimine-Catalyzed α-Olefins Polymerization: Thermoplastic Elastomers of Block Copolymers. *Macromolecules* **2015**, *48*, 1304−1312.
(30) Leone, G.; Losio, S.; Piovani, D.; Sommazzi, A.; Ricci, G. Living Copolymerization of Ethylene with 4-Methyl-1-Pentene by an α-Diimine Ni(II)/Et_2AlCl Catalyst: Synthesis of Diblock Copolymers via Sequential Monomer Addition. *Polym. Chem.* **2012**, *3*, 1987−1990.
(31) Gottfried, A. C.; Brookhart, M. Living and Block Copolymerization of Ethylene and α-Olefins Using Palladium(II)−α-Diimine Catalysts. *Macromolecules* **2003**, *36*, 3085−3100.
(32) O'Connor, K. S.; Watts, A.; Vaidya, T.; LaPointe, A. M.; Hillmyer, M. A.; Coates, G. W. Controlled Chain Walking for the Synthesis of Thermoplastic Polyolefin Elastomers: Synthesis, Structure, and Properties. *Macromolecules* **2016**, *49*, 6743−6751.
(33) Guan, Z. Control of Polymer Topology by Chain-Walking Catalysts. *Chem. - Eur. J.* **2002**, *8*, 3086−3092.
(34) McCord, E. F.; McLain, S. J.; Nelson, L. T. J.; Ittel, S. D.; Tempel, D.; Killian, C. M.; Johnson, L. K.; Brookhart, M. ^{13}C NMR Analysis of α-Olefin Enchainment in Poly(α-olefins) Produced with Nickel and Palladium α-Diimine Catalysts. *Macromolecules* **2007**, *40*, 410−420.
(35) Rose, J. M.; Cherian, A. E.; Lee, J. H.; Archer, L. A.; Coates, G. W.; Fetters, L. J. Rheological Behavior of Chain-Straightened Poly(α-olefin)s. *Macromolecules* **2007**, *40*, 6807−6813.
(36) Subramanyam, U.; Sivaram, S. Synthesis and Characterization of Poly(Higher-α-Olefin)s with a Nickel(α-Diimine)/Methylaluminoxane Catalyst System: Effect of Chain Running on the Polymer Properties. *J. Polym. Sci., Part A: Polym. Chem.* **2007**, *45*, 191−210.
(37) Johnson, L. K.; Killian, C. M.; Brookhart, M. New Pd(II)- and Ni(II)-Based Catalysts for Polymerization of Ethylene and α-Olefins. *J. Am. Chem. Soc.* **1995**, *117*, 6414−6415.
(38) Wang, Z.; Liu, Q.; Solan, G. A.; Sun, W.-H. Recent Advances in Ni-Mediated Ethylene Chain Growth: N_{imine}-Donor Ligand Effects on Catalytic Activity, Thermal Stability and Oligo-/Polymer Structure. *Coord. Chem. Rev.* **2017**, *350*, 68−83.
(39) O'Connor, K. S.; Lamb, J. R.; Vaidya, T.; Keresztes, I.; Klimovica, K.; LaPointe, A. M.; Daugulis, O.; Coates, G. W. Understanding the Insertion Pathways and Chain Walking Mechanisms of α-Diimine Nickel Catalysts for α-Olefin Polymerization: A ^{13}C NMR Spectroscopic Investigation. *Macromolecules* **2017**, *50*, 7010−7027.
(40) Meinhard, D.; Wegner, M.; Kipiani, G.; Hearley, A.; Reuter, P.; Fischer, S.; Marti, O.; Rieger, B. New Nickel(II) Diimine Complexes and the Control of Polyethylene Microstructure by Catalyst Design. *J. Am. Chem. Soc.* **2007**, *129*, 9182−9191.
(41) Vaidya, T.; Klimovica, K.; LaPointe, A. M.; Keresztes, I.; Lobkovsky, E. B.; Daugulis, O.; Coates, G. W. Secondary Alkene Insertion and Precision Chain-Walking: A New Route to Semicrystalline "Polyethylene" from α-Olefins by Combining Two Rare Catalytic Events. *J. Am. Chem. Soc.* **2014**, *136*, 7213−7216.
(42) Rhinehart, J. L.; Brown, L. A.; Long, B. K. A Robust Ni(II) α-Diimine Catalyst for High Temperature Ethylene Polymerization. *J. Am. Chem. Soc.* **2013**, *135*, 16316−16319.
(43) Liu, F.-S.; Hu, H.-B.; Xu, Y.; Guo, L.-H.; Zai, S.-B.; Song, K.-M.; Gao, H.-Y.; Zhang, L.; Zhu, F.-M.; Wu, Q. Thermostable α-Diimine Nickel(II) Catalyst for Ethylene Polymerization: Effects of the Substituted Backbone Structure on Catalytic Properties and Branching Structure of Polyethylene. *Macromolecules* **2009**, *42*, 7789−7796.
(44) Zou, W.; Chen, C. Influence of Backbone Substituents on the Ethylene (Co)polymerization Properties of α-diimine Pd(II) and Ni(II) Catalysts. *Organometallics* **2016**, *35*, 1794−1801.
(45) Zhong, L.; Li, G.; Liang, G.; Gao, H.-Y.; Wu, Q. Enhancing Thermal Stability and Living Fashion in α-Diimine−Nickel-Catalyzed (Co)polymerization of Ethylene and Polar Monomer by Increasing the Steric Bulk of Ligand Backbone. *Macromolecules* **2017**, *50*, 2675−2682.
(46) Camacho, D. H.; Guan, Z. Designing Late-Transition Metal Catalysts for Olefin Insertion Polymerization and Copolymerization. *Chem. Commun.* **2010**, *46*, 7879−7893.
(47) Song, K.; Yang, W.; Li, B.; Liu, Q.; Redshaw, C.; Li, Y.; Sun, W.-H. Nickel(II) Complexes Bearing 4,5-bis(arylimino)pyrenylidenes: Synthesis, Characterization, and Ethylene Polymerization Behavior. *Dalton Trans.* **2013**, *42*, 9166−9175.
(48) Yuan, J.; Wang, X.; Mei, T.; Liu, Y.; Miao, C.; Xie, X. An α-Diimine-Nickel(II) catalyst bearing an electron-withdrawing substituent for olefin polymerization. *Transition Met. Chem.* **2011**, *36*, 433−439.
(49) Liu, J.; Li, Y.; Li, Y.; Hu, N. Ethylene Polymerization by (α-Diimine)Nickel(II) Complexes Bearing Different Substituents on *para*-Position of Imines Activated with MMAO. *J. Appl. Polym. Sci.* **2008**, *109*, 700−707.
(50) Zhang, D.; Nadres, E. T.; Brookhart, M.; Daugulis, O. Synthesis of Highly Branched Polyethylene Using "Sandwich" (8-*p*-Tolyl naphthyl α-diimine)nickel(II) Catalysts. *Organometallics* **2013**, *32*, 5136−5143.
(51) Peleška, J.; Hoštálek, Z.; Hasalíková, D.; Merna, J. Living/Controlled Hex-1-ene Polymerization Initiated by Nickel Diimine Complexes Activated by non-MAO Cocatalysts: Kinetic and UV−vis Study. *Polymer* **2011**, *52*, 275−281.
(52) Merna, J.; Hoštálek, Z.; Peleška, J.; Roda, J. Living/Controlled Olefin Polymerization Initiated by Nickel Diimine Complexes: the Effect of Ligand Ortho Substituent Bulkiness. *Polymer* **2009**, *50*, 5016−5023.
(53) Gates, D. P.; Svejda, S. A.; Oñate, E.; Killian, C. M.; Johnson, L. K.; White, P. S.; Brookhart, M. Synthesis of Branched Polyethylene

Using (α-Diimine)nickel(II) Catalysts: Influence of Temperature, Ethylene Pressure, and Ligand Structure on Polymer Properties. *Macromolecules* **2000**, *33*, 2320−2334.
(54) Sheldrick, G. M. *SHELXTL Reference Manual*; Siemens Analytical X-ray Systems, Inc.: Madison, WI, 1996.
(55) Sheldrick, G. M. A Short History of SHELX. *Acta Crystallogr., Sect. A: Found. Crystallogr.* **2008**, *64*, 112−122.
(56) Azoulay, J. D.; Bazan, G. C.; Galland, G. B. Microstructural Characterization of Poly(1-hexene) Obtained Using a Nickel α-Keto-β-diimine Initiator. *Macromolecules* **2010**, *43*, 2794−2800.
(57) Simanke, A. G.; Alamo, R. G.; Galland, G. B.; Mauler, R. S. Wide-angle X-ray Scattering of Random Metallocene-Ethylene Copolymers with Different Types and Concentration of Comonomer. *Macromolecules* **2001**, *34*, 6959−6971.
(58) Gomes, C. S. B.; Gomes, P. T.; Duarte, M. T. α-Diimine Transition-Metal Complexes: Mechanochemistry − A New Synthetic Approach. *J. Organomet. Chem.* **2014**, *760*, 101−107.
(59) Allen, F. H. The Cambridge Structural Database: a Quarter of a Million Crystal Structures and Rising. *Acta Crystallogr., Sect. B: Struct. Sci.* **2002**, *58*, 380−388.
(60) Tempel, D. J.; Johnson, L. K.; Huff, R. L.; White, P. S.; Brookhart, M. Mechanistic Studies of Pd(II)−α-Diimine-Catalyzed Olefin Polymerizations. *J. Am. Chem. Soc.* **2000**, *122*, 6686−6700.
(61) Dai, S.; Zhou, S.; Zhang, W.; Chen, C. Systematic Investigations of Ligand Steric Effects on α-Diimine Palladium Catalyzed Olefin Polymerization and Copolymerization. *Macromolecules* **2016**, *49*, 8855−8862.
(62) Popeney, C. S.; Guan, Z. Effect of Ligand Electronics on the Stability and Chain Transfer Rates of Substituted Pd(II) α-Diimine Catalysts. *Macromolecules* **2010**, *43*, 4091−4097.
(63) Xiao, L.; Gao, R.; Zhang, M.; Li, Y.; Cao, X.; Sun, W.-H. 2-(1*H*-2-Benzimidazolyl)-6-(1-(arylimino)ethyl)pyridyl Iron(II) and Cobalt-(II) Dichlorides: Syntheses, Characterizations, and Catalytic Behaviors toward Ethylene Reactivity. *Organometallics* **2009**, *28*, 2225−2233.
(64) Zhang, M.; Wang, K.; Sun, W.-H. Chromium(III) complexes bearing 2-benzazole-1,10-phenanthrolines: synthesis, molecular structures and ethylene oligomerization and polymerization. *Dalton Trans.* **2009**, 6354−6363.
(65) Radlauer, M. R.; Day, M. W.; Agapie, T. Dinickel Bisphenoxyiminato Complexes for the Polymerization of Ethylene and α-Olefins. *Organometallics* **2012**, *31*, 2231−2243.
(66) Cotts, P. M.; Guan, Z.; McCord, E.; McLain, S. Novel Branching Topology in Polyethylenes As Revealed by Light Scattering and ^{13}C NMR. *Macromolecules* **2000**, *33*, 6945−6952.
(67) Hu, H.; Gao, H.; Chen, D.; Li, G.; Tan, Y.; Liang, G.; Zhu, F.; Wu, Q. Ligand-Directed Regioselectivity in Amine−Imine Nickel-Catalyzed 1-Hexene Polymerization. *ACS Catal.* **2015**, *5*, 122−128.
(68) Wang, H. P.; Chum, S. P.; Hiltner, A.; Baer, E. Deformation of Elastomeric Polyolefin Spherulites. *J. Polym. Sci., Part B: Polym. Phys.* **2009**, *47*, 1313−1330.
(69) Alizadeh, A.; Richardson, L.; Xu, J.; McCartney, S.; Marand, H.; Cheung, Y. W.; Chum, S. Influence of Structural and Topological Constraints on the Crystallization and Melting Behavior of Polymers. 1. Ethylene/1-Octene Copolymers. *Macromolecules* **1999**, *32*, 6221−6235.
(70) Bensason, S.; Minick, J.; Moet, A.; Chum, S.; Hiltner, A.; Baer, E. Classification of Homogeneous Ethylene-Octene Copolymers Based on Comonomer Content. *J. Polym. Sci., Part B: Polym. Phys.* **1996**, *34*, 1301−1315.
(71) Peeters, M.; Goderis, B.; Reynaers, H.; Mathot, V. Morphology of Homogeneous Copolymers of Ethylene and 1-Octene. II. Structural Changes on Annealing. *J. Polym. Sci., Part B: Polym. Phys.* **1999**, *37*, 83−100.
(72) Liu, W.; Zhang, X.; Bu, Z.; Wang, W. J.; Fan, H.; Li, B. G.; Zhu, S. Elastomeric Properties of Ethylene/1-Octene Random and Block Copolymers Synthesized From Living Coordination Polymerization. *Polymer* **2015**, *72*, 118−124.
(73) Wang, H. P.; Chum, S. P.; Hiltner, A.; Baer, E. Comparing elastomeric behavior of block and random ethylene−octene copolymers. *J. Appl. Polym. Sci.* **2009**, *113*, 3236−3244.
(74) Wang, H. P.; Khariwala, D. U.; Cheung, W.; Chum, S. P.; Hiltner, A.; Baer, E. Characterization of Some New Olefinic Block Copolymers. *Macromolecules* **2007**, *40*, 2852−2862.